Article:
Li, X, Ye, S orcid.org/0000-0001-5152-5753, Huang, Y et al. (2 more authors) (2019) Precise growth of polymer brushes on silica-based nanocomposites via visible-light-regulated controlled radical polymerization. Journal of Materials Chemistry A, 7 (11). pp. 6173-6179. ISSN 2050-7488

https://doi.org/10.1039/c9ta00905a

Precise Growth of Polymer Brushes on Silica-Based Nanocomposites via Visible-Light-Regulated Controlled Radical Polymerization

Xue Li,[a,b] Sunjie Ye,[c] Ya Huang,[a,b] Jia Le Li[a,b] and Tao Cai[a,b,*]

[a]Key Laboratory of Biomedical Polymers of Ministry of Education, College of Chemistry and Molecular Science, Wuhan University, Wuhan, Hubei 430072, P. R. China

[b]Wuhan University Shenzhen Research Institute, Shenzhen, Guangdong 518057, P. R. China

[c]School of Physics and Astronomy, University of Leeds, LS2 9JT, Leeds, UK

*Corresponding author.
Email address: chemcaitao@whu.edu.cn

Abstract

Precise control over molecular variables of grafted polymer brushes is of crucial importance for obtaining polymer nanocomposites with desirable architectures and physicochemical properties, yet it remains a significant synthetic challenge. Recent advances in photoinduced electron/energy transfer reversible addition fragmentation chain transfer (PET-RAFT) polymerization have enabled light-regulated polymer synthesis, in a well-controlled and environmentally friendly manner. However, the utilization of this modern synthetic technique towards the precise control of polymer brushes is underdeveloped. Here, PET-RAFT polymerization has been proceeded in a spatiotemporally controlled manner upon light regulation, producing silica nanocomposites coated with well-defined polymer brushes of target molecular weights, narrow dispersities and high grafting densities. The versatility and robustness of this technique have been demonstrated by its extendibility to other monomers and silica-containing nanomaterials. In all examined cases, the resultant high-value polymer nanocomposites possess defined chain sequences and architectures, high uniformity, and can be further expanded to a library of complex nanostructures. This work represents the first demonstration of adopting PET-RAFT approach for generating precisely-controlled polymer brushes on silica-based nanomaterials, and opens a new avenue for developing polymer nanocomposites with sequence-controlled polymer brushes and complex architectures required for a variety of target applications.

Keywords: Polymer nanocomposites, silica template, PET-RAFT polymerization, precipitation polymerization

Introduction

Inorganic/organic hybrid nanomaterials are an emerging and intriguing class of composite materials that can find wide applications in a variety of fields, including biology, catalysis and optics.[1-8] Structural synergy between the inorganic component and the macromolecular architecture broadens the window of physicochemical properties of common nanomaterials and thereby enriches their function and application spectrum. These prospective combinations boost the exploration of appropriate polymer coatings onto the inorganic nanomaterials to confer synergistic properties such as processability, flexibility, multi-stimuli responsiveness, biocompatibility and stability in a variety of solvents without the intervention of redesigning the inorganic components. Several approaches, including physical adsorption, self-assembly, covalent attachment or layer-by-layer techniques, have been proposed to synthesize these hybrid nanomaterials.

Polymer brushes are three-dimensional molecular architectures in which concentrated polymer chains are linked to one side of a solid substrate and therefore the end-tethered chains are forced to stretch away from the surface.[9] Previous reports have indicated that precise control over molecular variables of the grafted polymer brushes including chain length, chain dispersity, macroscopic structure and grafting density, is of crucial importance to comprehend and optimize the dispersion state, strength of interaction, and myriads of physicochemical properties of the resultant polymer nanocomposites.[10,11] Nonetheless, among the methodologies developed for constructing polymer brushes, surface-initiated controlled radical polymerization is regarded as the most promising technique to fulfill the aforementioned requirements, where an initiator or chain transfer agent (CTA) is preliminarily linked to the nanomaterials and attached polymer brushes

are propagated from the modified surfaces.[12-14] In the pursuit of solar-driven synthesis of natural polymers with well-preserved chain terminus fidelity as well as composition, spatiotemporal and sequence control, extensive research has been devoted to the development and exploitation of visible-light-mediated modern polymer synthesis for precise control over the polymerization procedures.[15-24] Arising from its highly advantageous characteristics including low cost, user-friendly operation, fast initiation efficiency and convenient spatiotemporal polymerization modulation, photoinduced electron/energy transfer reversible addition fragmentation chain transfer (PET-RAFT) polymerization enables a versatile toolkit for controlled polymerizations of diverse functional monomers from nanomaterials and is universal in its specificity to satisfy the energetic criteria for conducting such polymerization, which would be otherwise inaccessible by thermal counterparts.[25-29]

To the best of our knowledge, the current work is the first example to illustrate a systematic method to propagate well-defined polymer brushes directly from the surface of various silica-assisted nanomaterials using a PET-RAFT approach. The effects of photocatalyst concentration and light irradiation time on the polymerization kinetics, monomer conversion, molecular weight distribution, grafting density, and shell thickness of the surface-linked polymer brushes were investigated. In addition, various silica-assisted nanomaterials such as Pt@SiO_2-PDP and Fe_3O_4@*a*SiO_2-PDP were also used as core particles to be grafted with a concentrated polymer brush in order to verify the versatility and applicability of the whole procedures from the fixation of CTA to the graft polymerization.

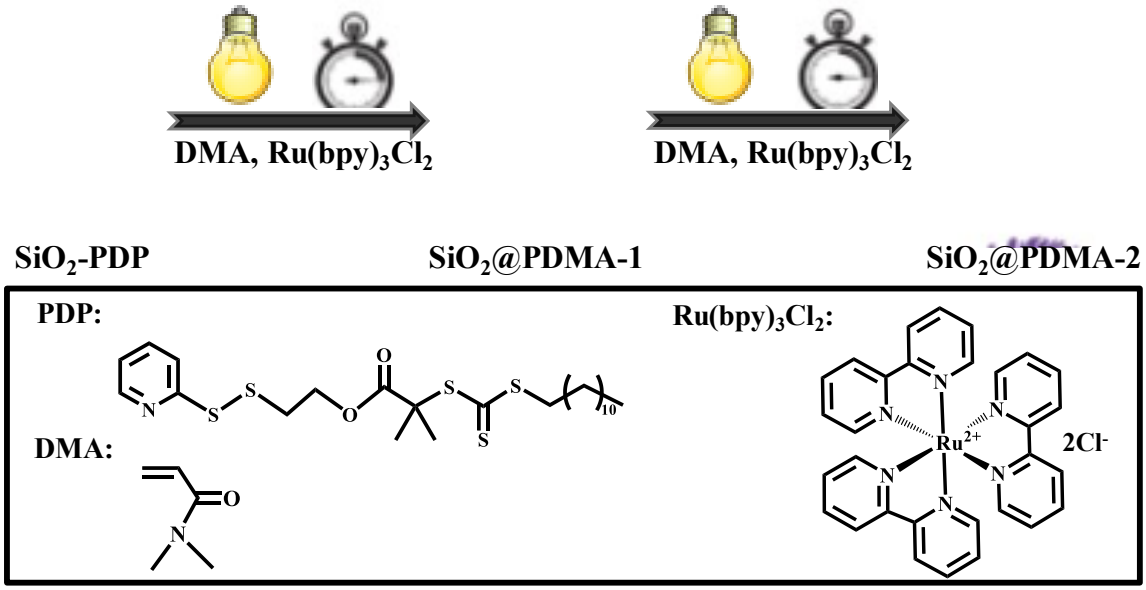

Scheme 1. Surface-initiated PET-RAFT polymerization of DMA monomers from SiO_2-PDP nanoparticles in acetonitrile with prior deoxygenation at 25 ºC under blue LED light irradiation.

Results and Discussion

In an effort to address the challenge for the characterization of real molecular weights and polydispersity of the surface-linked polymer brushes, a thiol-reactive CTA, 2-(pyridine-2-yldisulfanyl)ethyl 2-(((dodecylthio)carbonthioyl)thio) propanoate (PDP) was preliminarily synthesized via esterification reaction of *S*-dodecyl-*S*′-(α,α′-dimethyl-α′′-acetic acid)trithiocarbonate with hydroxyethyl pyridyldisulfide. Detailed information about the synthesis and characterization of PDP is provided in Supplementary Information (Scheme S1 and Figure S1). Narrowly dispersed CTA-anchored silica composite nanoparticles (SiO_2-PDP NPs) with a diameter of 145 ± 10 nm was fabricated via an ammonia-catalyzed hydrolysis/condensation process of tetraethyl orthosilicate (TEOS) and 3-(mercaptopropyl) trimethoxysilane (MPTMS), follow by thiol-disulfide exchange reaction between SiO_2-MPTMS and PDP to anchor the trithiocarbonate moieties on the surface.[29,30] The amount of CTAs fixed on the substrate is a vital parameter as it presents the upper limit on the grafting density of the resultant polymer brushes.[12-14] Considering the remaining weight percentage after disulfide cleavage, the average size of SiO_2-PDP NPs (145 nm), and assuming that the density of silica NPs was identical to that of bulk silica (2.07 g/cm^3), the density of CTA units on silica NPs were estimated to be 4.4×10^{-5} mol PDP per 1.0 mg of SiO_2-PDP NPs or 1.34 units per nm^2 (Table S1).[12-14] The successful immobilization of PDP on the silica NP surfaces was clearly established using an X-ray photoelectron spectroscopy (XPS) wide scan profile, where the emergence of N 1s and S 2p signals was evident, as displayed in Figure 1a.

A major issue in the surface-initiated polymerization for forming polymer brushes lies in the undesirable gelation or particle aggregation arising from the unpredictable

polymerization process form nanosized particles especially in the construction of thick polymer layers. This can be effectively solved via the strategy of precipitation polymerization, in which the modified polymer nanocomposites formed by propagation of respective monomers and/or crosslinkers would eventually separate out of the original homogeneous suspension owing to the low solubility of the newly fabricated polymer brushes with low solubility in the specific reaction media.[29,30] To this end, the selection of solvent is of paramount importance. In our present study, we have judiciously chosen acetonitrile, owing to its low boiling point, good solubility of a myriad of monomers and $Ru(bpy)_3Cl_2$ photocatalyst, good dispersibility of the starting CTA-fixed silica-based NPs and yet poor dispersibility of most of the resultant polymer nanocomposites.[31-33] Moreover, it has been widely reported that higher dielectric constant of the solvents can afford favorable stabilization to the radical intermediates and in return promote the polymerization kinetics. Obviously, the current technique broadened the monomer pool in radical polymerizations and significantly mitigated the undesirable side reactions including accelerated radical transfer to solvents and impurities and degradation of CTA.[31-33]

Surface-initiated PET-RAFT polymerization of *N,N*-dimethylacrylamide (DMA) from SiO_2-PDP NPs with three different $Ru(bpy)_3Cl_2$ concentrations of 75 ppm, 50 ppm and 25 ppm (in relation to molar ratio of monomer), was conducted in acetonitrile under blue LED light irradiation (4.8 W, λ_{max} = 465 nm, 1.0 mW/cm^2), as displayed in Scheme 1. In order to maintain the same polymerization conditions, the molar feed ratio of [DMA]:[PDP] was set at 2000:1 unless otherwise indicated. Reductive scission of the

disulfide linkages in the respective SiO_2@PDMA core-shell NPs in predetermined time intervals was performed using excessive tris(2-carboxyethyl)phosphine (TCEP) to obtain the detached thiol-terminated PDMA chains. The cleaved polymer brushes were collected by vacuum drying and monitored by ^{1}H NMR and GPC (Figures S2 and S3). A linear relationship of $\ln[M]_0/[M]_t$ against exposure time t corresponds to a pseudo first-order polymerization kinetics, as demonstrated in Figure 1b. Obviously, the deduced apparent propagation rate constants (k_p) from linear fitting of the results in Figure 1b increased from 0.10 h^{-1} to 0.23 h^{-1} with increasing photocatalyst loading from 25 to 75 ppm. It is worth mentioning that k_p in the current surface-initiated PET-RAFT polymerization system was found to be much lower than that in the case using sacrificial CTAs under an identical polymerization condition, probably arising from the constrained propagation access of monomers to the surface-fixed CTA in a diluted mode.[14,34] Temporal control was utilized by iterative activation and deactivation of polymerizations in programmable "ON/OFF" experiments (Figure 1c). Switching off the light completely suppressed the polymerization and the system was dormant in dark, whereas switching on the light steadily resumed original linear chain propagation. As verified by GPC elution traces, the polymerization of DMA demonstrated optimal control over molecular weight distribution (polydispersity index $Đ < 1.20$) at this photocatalyst concentration, though the molecular weights derived from GPC ($M_{n,GPC}$) were greater than those derived from ^{1}H NMR ($M_{n,NMR}$) in all occasions, which was attributed to the use of linear poly(ethylene oxide) (PEO) standards for the GPC calibration (Figures 1d and S3). By considering the weight percentage of the detached thiol-terminated PDMA chains, the average size of CTA-anchored silica NPs (145 nm), the grafting density of PDMA brushes on silica NPs was

calculated to be in the range of 0.30-0.36 chains/nm^2 (Table S1), which is comparable to those reported in the literature.[9,12-14] The monomer diffusion to the available initiation sites can be restricted or even sheltered by the existing grafted polymer brushes, and this effect becomes more remarkable with prolonged exposure time, leading to a significant loss of CTAs for the initiation of polymerization and a slight decline of grafting density with increasing the chain length of polymer brushes.[9,12-14]

The PDMA shell thickness can be easily tuned via regulation of irradiation time during PET-RAFT polymerization. The TEM images (Figures 1e, 1f and 1g) clearly show a uniform and smooth macromolecular corona with various shell-thickness surrounding a solid nanocore. The PDMA shell obtained within the initial 0.5 h possessed a thickness of 6.1 ± 0.8 nm, and an additional 1 h yielded a shell thickness of 15.8 ± 1.7 nm. Further increase of exposure time to around 4 h led the PDMA shell to reach the thickness limit of 39.8 ± 3.3 nm, as the SiO_2@PDMA-3 NPs would precipitate out of the reaction media. It is conceivable that the PDMA shell thickness exhibited a linear dependency on monomer conversions (Figure 1c). The wide-scan spectra from XPS measurement (Figure 1a) displayed an enhanced N 1s signal and substantially weakened or even diminished Si 2p signal, due to the limited XPS sampling depth of organic matrices of around 10 nm. The spectra changes corroborate the successful chain extension at predetermined time intervals. The curve-fitted XPS C 1s core-level spectrum of the SiO_2@PDMA-2 NPs split into three peak components with binding energies (BEs) at 284.6, 285.6 and 287.4 eV coupled with an approximate spectral area ratio of 2.1:2:1, attributable to the -C-C/-CH-, -C-N- and -N-C=O species, respectively, in accordance

with the chemical structure of neat PDMA polymer (Figure S4).[9,12-14] Figure S5 exhibited the thermal degradation behaviors of PDMA polymer, SiO_2-PDP and three SiO_2@PDMA NPs by TGA. Differing from the SiO_2-PDP starting NPs with an ambiguous major weight loss in the whole procedure, all the SiO_2@PDMA NPs and PDMA polymer possessed an exclusive major weight loss occurring at around 350 ºC when gradually increasing the temperature to 700 ºC. However, the continuous release of labile substances entrapped inside the silica NPs during the TGA measurement made it inappropriate for the calculation of corresponding grafting density.

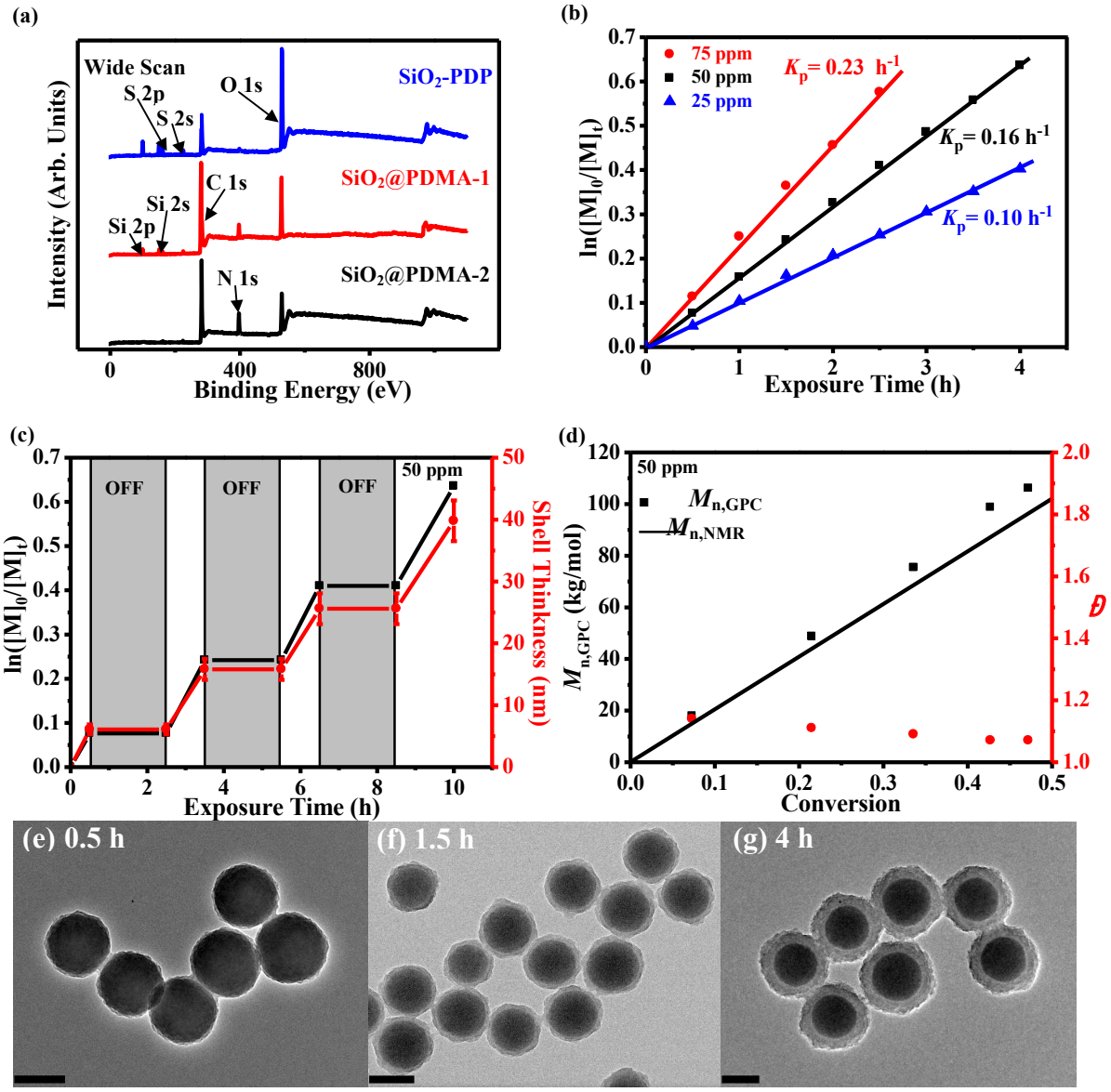

Figure 1. Surface-initiated PET-RAFT polymerization of DMA monomers from SiO_2-PDP nanoparticles in acetonitrile with prior deoxygenation at 25 ºC under blue LED light irradiation (4.8 W, λ_{max} = 465 nm, 1.0 mW/cm^2). (a) XPS wide-scan spectra of SiO_2-PDP, SiO_2@PDMA-1 and SiO_2@PDMA-2 nanoparticles; (b) plot of $\ln[M]_0/[M]_t$ versus exposure time t at three different $Ru(bpy)_3Cl_2$ concentrations in reference to monomer concentration; (c) temporal control over polymerization upon on/off switches of light and (d) evolution of $M_{n,NMR}$, $M_{n,GPC}$ and $Đ$ versus monomer conversion. TEM images of (e) SiO_2@PDMA-1, (f) SiO_2@PDMA-2 and (g) SiO_2@PDMA-3 nanoparticles. All scale bars are 100 nm.

Seeking to broaden the application prospect and access the chemical versatility and robustness of $Ru(bpy)_3Cl_2$ as the photocatalyst, we investigated surface-initiated PET-RAFT polymerization of *N*-isopropylacrylamide (NIPAM) from Pt@SiO_2-PDP core-shell NPs in acetonitrile. The Pt@SiO_2-PDP core-shell NPs with a diameter of 62 ± 3 nm were fabricated according to our previous procedures (Figure S6).[35] Reversible activation and deactivation upon manipulating intermittent cycles of light and dark allowed highly fine-regulated and effective control over the shell thickness on the silica surface despite the original composition and architecture of silica-based nanocomposites. The temporal control of this process was estimated by keeping the light source off for 2 h at the predetermined time intervals of 0.5, 3 and 6 h (Figure 2a). Switching off the light spontaneously halted the polymerization and the system was dormant in dark, whereas switching on the light steadily resumed original linear chain propagation. The good accordance between the molecular weights $M_{n,NMR}$ and $M_{n,GPC}$ of the cleaved PNIPAM homopolymers as well as the gradual decrease in polydispersities ($Đ$) with elevating monomer conversions even following multiple on/off runs (Figure 2b), substantiated the high end-group fidelity and the living feature of the process. It is noteworthy that the observed $M_{n,GPC}$ was identified to be slightly overestimated, which was ascribed to the calibration with PEO reference polymers.

The PNIPAM shell thickness for the polymer-grafted core-double-shell nanostructure can be smoothly controlled by the modulation of light exposure time in the PET-RAFT approach. The TEM images of Figure 2e and 2f revealed a dense Pt@SiO_2 core-shell NP of deeper contrast encircled by a spherical polymer scaffold of a differential contrast,

yielding an elegant core-double-shell hybrid nanostructure. With the increase of exposure time, the PNIPAM shell thickness increases correspondingly from 5.8 ± 0.5 nm at 0.5 h, to 11.8 ± 1.2 nm at 1 h and to 29.3 ± 2.4 nm at 3 h (Figure 2a). The enhanced intensity of N element in the XPS wide-scan spectrum vindicated the existence of PNIPAM adducts on the silica interlayer (Figure 2c). Additional information on the molecular structure of Pt@SiO_2@PNIPAM-2 NPs was obtained from the curve-fitted XPS C 1s core-level spectrum. It split into three peak components with BEs at 284.6, 285.6 and 287.4 eV and with an approximate spectral area ratio of 4:1:1, attributable to the -C-C/-CH-, -C-N- and -N-C=O species, respectively, consistent with the chemical structure of neat PNIPAM polymer (Figure S7).[9,12-14]

In a parallel experiment, a crosslinking agent, ethylene glycol dimethacrylate (EGDMA, 15 mol% relative to NIPAM) was introduced to reaction mixture to solidify the PNIPAM exterior shell, after which the silica sacrificial layer in the Pt@SiO_2@PNIPAM core-double-shell NPs can be completely eroded by hydrofluoric acid treatment to generate the Pt@*h*PNIPAM hybrid nanorattles. The PNIPAM shell thickness of 11.8 nm with a high crosslinking degree confers sufficient strength to withstand the external destruction, affording the Pt@*h*PNIPAM hybrid nanorattles with donut-like biconcave morphology free of visible defects, as shown in the TEM image (Figure 2g). The PNIPAM shell bestowed Pt@*h*PNIPAM-2 hybrid nanorattles with thermosensitive characteristics, as verified by the decline of corresponding hydrodynamic diameter (D_h) upon elevating the solution temperature in dynamic light scattering (DLS) analysis, with the most pronounced alteration being detected in the temperature range of 25-35 ºC (Figure 2d).

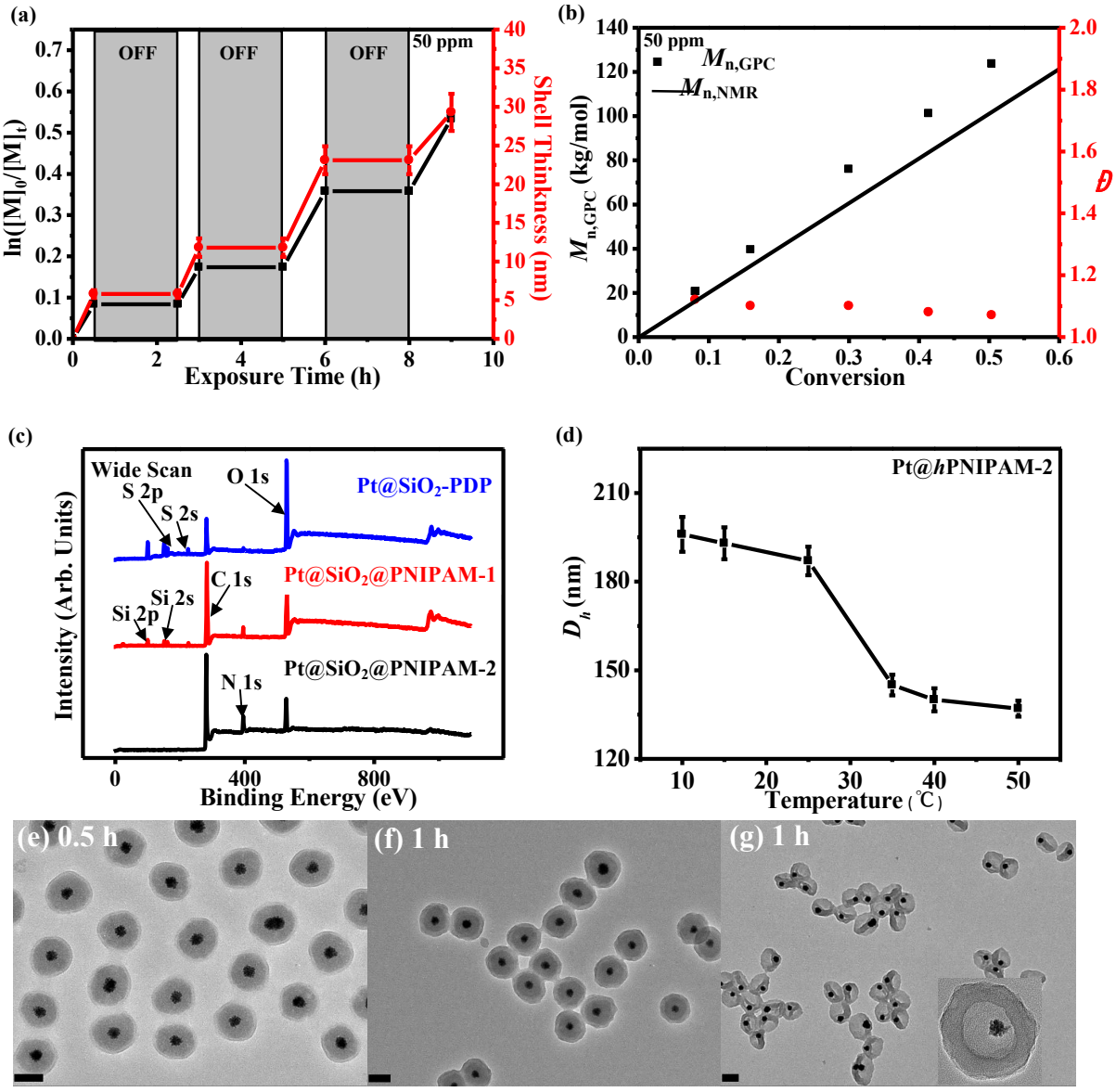

Figure 2. Surface-initiated PET-RAFT polymerization of NIPAM monomers from Pt@SiO_2-PDP nanoparticles in acetonitrile with prior deoxygenation at 25 ºC under blue LED light irradiation (4.8 W, λ_{max} = 465 nm, 1.0 mW/cm^2). (a) Temporal control over polymerization upon on/off switches of light; (b) evolution of $M_{n,NMR}$, $M_{n,GPC}$ and $Đ$ versus monomer conversion; (c) XPS wide-scan spectra of Pt@SiO_2-PDP, Pt@SiO_2@PNIPAM-1 and Pt@SiO_2@PNIPAM-2 nanoparticles, and (d) influence of increasing temperature on the hydrodynamic diameters (D_h) of the Pt@*h*PNIPAM-2 nanoparticles in aqueous media. TEM images of (e) Pt@SiO_2@PNIPAM-1, (f) Pt@SiO_2@PNIPAM-2 and (g) Pt@*h*PNIPAM-2 nanoparticles. All scale bars are 50 nm.

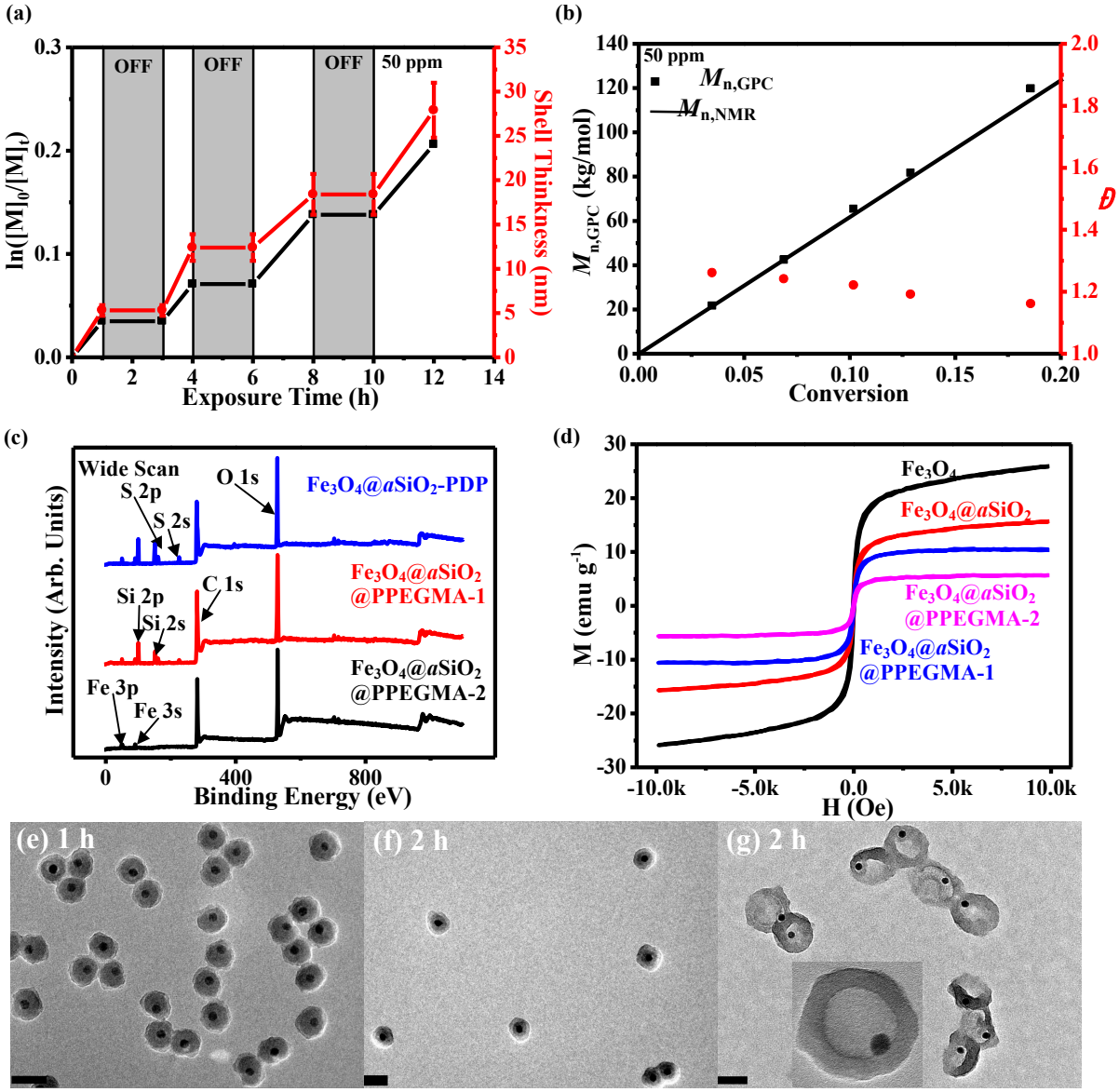

Figure 3. Surface-initiated PET-RAFT polymerization of PEGMA monomers from Fe_3O_4@$a$$SiO_2$-PDP nanoparticles in acetonitrile with prior deoxygenation at 25 ºC under blue LED light irradiation (4.8 W, λ_{max} = 465 nm, 1.0 mW/cm^2). (a) Temporal control over polymerization upon on/off switches of light; (b) evolution of $M_{n,NMR}$, $M_{n,GPC}$ and $Đ$ versus monomer conversion; (c) XPS wide-scan spectra and (d) field-dependent magnetization of Fe_3O_4, Fe_3O_4@$a$$SiO_2$-PDP, Fe_3O_4@$a$$SiO_2$@PPEGMA-1 and Fe_3O_4@$a$$SiO_2$@PPEGMA-2 nanoparticles. TEM images of (e) Fe_3O_4@$a$$SiO_2$@PPEGMA-1, (f) Fe_3O_4@$a$$SiO_2$@PPEGMA-2 and (g) Fe_3O_4@hPPEGMA-2 nanoparticles. All scale bars are 50 nm.

One of the advantages of visible-light-regulated polymerization is the capability to carry out reactions under mild conditions which is especially attractive in terms of retaining control over polymerization of labile monomers at high temperature. Intrigued by the high efficiency of $Ru(bpy)_3Cl_2$ mediated PET-RAFT polymerization, we further extended this grafting technique to another silica-based nanocomposites, by performing surface-initiated PET-RAFT polymerization of poly(ethylene glycol) methyl ether methacrylate (PEGMA, M_n = 300 g/mol) from Fe_3O_4@*a*SiO_2-PDP Janus NPs in a concurrent experiment with an identical procedure. The Fe_3O_4@*a*SiO_2-PDP Janus NPs with a silica hemisphere of 35 ± 2 nm in diameter were synthesized according to our previous procedure (Figure S8).[36] Figure 3a shows the evolution of the polymer thickness grafted on the silica interlayer upon temporal control by exposure to an alternating sequence of visible light on and off environment with a time interval of 2 h. No monomer consumption was detected in the dark period whilst the polymerization proceeded as expected in the irradiated period. The evident transformations to higher $M_{n,GPC}$ of the detached PPEGMA homopolymers were detected in the GPC elusion curves with trivial tailing or coupling. The corresponding narrow distributions were retained with increasing monomer conversions (Figure 3b), thus further highlighting the versatility and robustness of this methodology.

A Janus nanostructure, in which a partially-buried Fe_3O_4 nanocore protruded from the silica nanosphere, had been gradually covered by the dense and thick polymer corona under prolonged light exposure, as displayed by TEM in Figure 3e and 3f, respectively. The PPEGMA shell thickness of 5.3 ± 0.6 nm was observed at a polymerization time of 1

h and it would increase to 12.4 ± 1.5 nm when the polymerization time of 2 h was applied. The shell thickness of Fe_3O_4@*a*SiO_2@PPEGMA NPs exceeded the probing depth (10 nm) of the XPS technique in organic matrices, which resulted in the signal elimination of distinctive S and Si elements in the XPS wide scan spectra (Figure 3c).[9,12-14] Concomitantly, the C 1s core-level spectrum was composed of three peak components with respective BEs at 284.6, 286.2 and 288.5 eV and the spectral area ratio approximates 3.2:10:1, attributable to the -C-C/-CH-, -C-O- and -O-C=O species, in good agreement with the chemical structure of PPEGMA polymer edges (Figure S9). These results cooperatively reveal that PET-RAFT polymerization provides an ideal route for controlled polymerization of various monomers from silica-based nanomaterials with precise control over the chain length or shell thickness through the adoption of visible light source as the regulator.

In addition, the adoption of EGDMA crosslinkers in a parallel experiment allow the subsequent selective elimination of the silica sacrificial layer by NaOH treatment to generate the Fe_3O_4@*h*PPEGMA polymer nanocomposites. The PPEGMA shell with thickness of 12.4 nm as well as a high crosslinking degree established a stable and rigid fortress to sustain the inner cavity, affording the Fe_3O_4@*h*PPEGMA hybrid NPs with delicate rattle-type nanostructure (Figure 3g). The magnetic properties are one of the paramount attributes for the design of Fe_3O_4-based NPs. Figure 3d demonstrates the respective field-dependent magnetization of the oleic acid-capped Fe_3O_4, Fe_3O_4@*a*SiO_2-PDP, Fe_3O_4@*a*SiO_2@PPEGMA-1 and Fe_3O_4@*a*SiO_2@PPEGMA-2 NPs. No hysteresis loops were detected for all the involved NPs and the order of saturation magnetization

value of different NPs is given by Fe_3O_4@*a*SiO_2@PPEGMA-2 NPs (~5.7 emu/g) < Fe_3O_4@*a*SiO_2@PPEGMA-1 NPs (~10.5 emu/g) < Fe_3O_4@*a*SiO_2-PDP NPs (~15.6 emu/g) < oleic acid-stabilized Fe_3O_4 NPs (~25.8 emu/g).[36] This discrepancy was probably associated with the increased interparticle distances from the PPEGMA polymer brushes and silica interlayers, and reduced concentration of Fe_3O_4 components.

Conclusion

In summary, surface-initiated PET-RAFT polymerization of DMA from SiO_2-PDP NPs was accomplished with excellent control over the molecular weight and dispersity of the graft polymer brushes, spatiotemporal regulation upon visible light and a high grafting density exceeding 0.3 chains/nm^2. The current strategy mediated by PET-RAFT polymerization was successfully extended to other monomers in tandem with silica-assisted Pt@SiO_2 core-shell and Fe_3O_4@*a*SiO_2 Janus nanomaterials as solid substrates. The resultant high-value polymer nanocomposites possessed well-defined chain sequences and architectures, high uniformity and outstanding dispersibility, and can be further converted to a library of complex nanostructures through the addition of crosslinkers during the polymerization and removal of the silica sacrificial layers thereafter. The user-friendly feature of our method expands the synthetic scope of various silica-based polymer nanocomposites coated with intriguing polymer brushes for diverse applications of precise nanomaterials design.

Acknowledgements: The financial support from the National Natural Science Foundation of China (51773156 and 51703167), the Science and Technology Program of Shenzhen (JCYJ20170303170403122 and JCYJ20170303170340122), the Natural Science Foundation of Jiangsu Province (BK20160384 and BK20170412), the Natural Science Foundation of Hubei Province (2017CFB127) and the Fundamental Research Funds for the Central Universities, China, administered by Wuhan University (Project No. 2042018kf0001) is acknowledged.

References

[1] R. Ciriminna, A. Fidalgo, V. Pandarus, F. Beland, L. M. Ilharco and M. Pagliaro, *Chem. Rev.*, 2013, **113**, 6592-6620.

[2] X. Wang, J. Feng, Y. Bai, Q. Zhang and Y. Yin, *Chem. Rev.*, 2016, **116**, 10983-11060.

[3] J. Gaitzsch, X. Huang and B. Voit, *Chem. Rev.*, 2016, **116**, 1053-1093.

[4] Y. Zhang, B. Y. W. Hsu, C. Ren, X. Li and J. Wang, *Chem. Soc. Rev.*, 2015, **44**, 315-335.

[5] S. K. Kumar, B. C. Benicewicz, R. A. Vaia and K. I. Winey, *Macromolecules*, 2017, **50**, 714-731.

[6] S. K. Kumar and N. Jouault, *Macromolecules*, 2013, **46**, 3199-3214.

[7] B. Zhang, T. Cai, S. Li, X. Zhang, Y. Chen. K. G. Neoh, E. T. Kang and C. Wang, *J. Mater. Chem. C.*, 2014, **2**, 5189-5197.

[8] T. Cai, B. Zhang, Y. Chen, C. Wang, C. X. Zhu, K. G. Neoh and E. T. Kang, *Chem. Eur. J.*, 2014, **20**, 2723-2731.

[9] J. O. Zoppe, N. C. Ataman, P. Mocny, J. Wang, J. Moraes and H. -A. Klok, *Chem. Rev.*, 2017, **117**, 1105-1318.

[10] W. Chen, R. Cordero, R.; H. Tran and C. K. Ober, *Macromolecules*, 2017, **50**, 4089-4113.

[11] S. Milner, *Science*, 1991, **251**, 905-914.

[12] A. Bagheri, H. Arandiyan, N. N. M. Adnan, C. Boyer and M. Lim, *Macromolecules*, 2017, **50**, 7137-7147.

[13] M. Sokolowski, C. Bartsch, V. J. Spiering, S. Prevost, M. -S. Appavou, R. Schweins and M. Gradzielski, *Macromolecules*, 2018, **51**, 6936-6948.

[14] K. Ohno, Y. Ma, Y. Huang, C. Mori, Y. Yahata, Y. Tsujii, T. Maschmeyer, J. Moraes and S. Perrier, *Macromolecules*, 2011, **44**, 8944-8953.

[15] X. Pan, M. A. Tasdelen, J. Laun, T. Junkers, Y. Yagci and K. Matyjaszewski, *Prog. Polym. Sci.*, 2016, **62**, 73-125.

[16] M. Chen, S. Deng, Y. Gu, J. Lin, M. J. MacLeod and J. A. Johnson, *J. Am. Chem. Soc.*, 2017, **139**, 2257-2266.

[17] M. Chen, M. Zhong and J. A. Johnson, *Chem. Rev.*, 2016, **116**, 10167-10211.

[18] B. P. Fors and C. J. Hawker, *Angew. Chem. Int. Ed.*, 2012, **51**, 8850-8853.

[19] N. J. Treat, H. Sprafke, J. W. Kramer, P. G. Clark, B. E. Barton, J. Read de Alaniz, B. P. Fors and C. J. Hawker, *J. Am. Chem. Soc.*, 2014, **136**, 16096-16101.

[20] J. Niu, D. J. Lunn, A. Pusuluri, J. I. Yoo, M. A. O'Malley, S. Mitragotri, H. T. Soh and C. J. Hawker, *Nat. Chem.*, 2017, **9**, 537-545.

[21] V. Kottisch, Q. Michaudel and B. P. Fors, *J. Am. Chem. Soc.*, 2017, **139**, 10665-10668.

[22] Q. Michaudel, V. Kottisch and B. P. Fors, *Angew. Chem. Int. Ed.*, 2017, **56**, 9670-9679.

[23] C. Wu, N. Corrigan, C. -H. Lim, K. Jung, J. Zhu, G. Miyake, J. Xu and C. Boyer, *Macromolecules*, 2019, **52**, 236-248.

[24] J. P. Cole, C. R. Federico, C. -H. Lim and G. M. Miyake, *Macromolecules*, 2019, **52**, 747-754.

[25] J. Yeow, S. Josh, R. Chapman and C. Boyer, *Angew. Chem. Int. Ed*., 2018, **57**, 10102-10106.

[26] N. Corrigan, S. Shanmugam, J. Xu and C. Boyer, *Chem. Soc. Rev.*, 2016, **45**, 6165-6212.

[27] A. J. Gormley, J. Yeow, G. Ng, O. Conway, C. Boyer and R. Chapman, *Angew. Chem. Int. Ed.*, 2018, **57**, 1557-1562.

[28] S. Shanmugam, S. Xu, N. N. M. Adnan and C. Boyer, *Macromolecules*, 2018, **51**, 779-790.

[29] Y. Huang, X. Li, J. L. Li, B. Zhang and T. Cai, *Macromolecules*, 2018, **51**, 7974-7982.

[30] G. L. Li, H. Mohwald and D. G. Shchukin, *Chem. Soc. Rev.*, 2013, **42**, 3628-3646.

[31] J. Xu, K. Jung, N. A. Corrigan and C. Boyer, *Chem. Sci.*, 2014, **5**, 3568-3575.

[32] J. Xu, K. Jung and C. Boyer, *Macromolecules*, 2014, **47**, 4217-4229.

[33] J. Yeow, J. Xu and C. Boyer, *ACS Macro Lett.*, 2015, **4**, 984-990.

[34] C. Bao, S. Tang, J. M. Horton, X. Jiang, P. Tang, F. Qiu, L. Zhu and B. Zhao, *Macromolecules*, 2012, **45**, 8027-8036.

[35] X. Li, T. Cai and E. T. Kang, *Macromolecules*, 2016, **49**, 5649-5659.

[36] X. Li, J. L. Li, W. G. Huang, X. Z. Zhang, B. Zhang and T. Cai, *Nanoscale*, 2018, **10**, 19254-19261.

For Table of Contents Use Only